

## COMMUNICATION

View Article Online  
View Journal | View Issue



Cite this: *Nanoscale Adv.*, 2020, 2, 1046

Received 8th December 2019  
Accepted 10th February 2020

DOI: 10.1039/c9na00769e

rsc.li/nanoscale-advances

Nanocrystal–ligand interactions deciphered: the influence of HSAB and  $pK_a$  in the case of luminescent ZnO†

Yohan Champouret,<sup>‡a</sup> Grégory Spataro,<sup>‡a</sup> Yannick Coppel,<sup>a</sup> Fabienne Gauffre <sup>\*b</sup> and Myrtil L. Kahn <sup>\*a</sup>

Despite all the efforts made by the scientific community to rationalize the interaction of organic molecules with nanocrystals (Ncs), we are still at the level of the empirical recipe when the material behavior in solution is concerned. In an effort to address this issue, the analysis of the luminescence measurements of ZnO Ncs in the presence of various organic substrates using a Langmuir adsorption model was carried out to determine for the first time the affinity constants and the number of binding sites as well as to rank the interaction strengths of these substrates with regard to ZnO Ncs. The results were confirmed by NMR spectroscopic studies, which, besides, provided a deep understanding of the substrate–ZnO Nc interactions. Analysis of the results using  $pK_a$  and HSAB theory demonstrates that the interaction of a given substrate can be determined by its  $pK_a$  versus the  $pK_a$  of the organic molecules present at the surface of pristine Ncs and that the hard or soft character of the substrates can govern the emission intensity of the ZnO Ncs.

The bibliography abounds with many examples of NPs of different natures (metallic, II–VI, and III–V) functionalized with different types of ligands such as amines, carboxylic acids, thiols, phosphines or phosphine oxides.<sup>5</sup> However, it must be noted that despite all the efforts made by the scientific community in this field, we are still at the level of the empirical recipe, a result of many trials and errors. Rationalization leading to prediction has not yet emerged.

One way to address this issue is to adopt a systematic approach for a given system that will provide access to the necessary fundamental data. These are of two types. On the one hand, there is physical–chemical information such as affinity constants and the number of binding sites and, on the other hand, there is information at the molecular level such as the specific sites of interactions of the ligand as well as their dynamics of binding/unbinding.

For more than 15 years, we have been working on the synthesis of nanoparticles using an organometallic approach.<sup>6</sup> In particular, this method provides access to ZnO nanocrystals (Ncs) stabilized by alkyl amines, forming stable colloids. An earlier NMR spectroscopy study allowed us to describe very precisely how alkylamines interact with ZnO Ncs and the dynamical aspects of these interactions.<sup>7</sup> This is therefore an ideal model system to initiate a systematic study, allowing us to establish a chemical affinity scale of different ligands for this type of nanoparticle.

In this work, we used the luminescence properties of ZnO to determine affinity constants and the number of binding sites. In addition, a quantitative NMR study was carried out to characterize the structural and dynamical aspects of the interactions between ligands and the Ncs. The surface modifications caused by the addition of another ligand (also called substrate) in the environment were thus clearly demonstrated. As ligands, we selected alkyl-thiols (octanethiol and dodecanethiol), phosphonic acids (hexyl- and tetradecyl-phosphonic acid), a ketone (hexan-2-one), an aldehyde (hexanal), an alcohol (1-octanol), and a carboxylic acid (lauric acid) which include the most widely used ligands that, in addition, expectedly present a wide

## Introduction

When nanoparticles (NPs) are prepared in solution, stabilizing agents, also known as ligands, are introduced into the reaction medium to ensure colloidal stability and control of the size and shape of the NPs. Post-functionalization of NPs might also be required.<sup>1</sup> It is then necessary to proceed with an exchange of ligands, while avoiding flocculation of the medium.<sup>2</sup> The ligand can also affect the intrinsic NP properties,<sup>3</sup> particularly, optical properties.<sup>4</sup> It should therefore be chosen with great care.

<sup>a</sup>Laboratoire de Chimie de Coordination UPR8241, CNRS, 205 Rte de Narbonne, 31000 Toulouse Cedex 04, France. E-mail: myrtil.kahn@lcc-toulouse.fr

<sup>b</sup>Univ Rennes, CNRS, ISCR-UMR6226, F-35000 Rennes, France. E-mail: fabienne.gauffre@univ-rennes1.fr

<sup>†</sup> Electronic supplementary information (ESI) available: 2D plot analysis, optical characterization, luminescence properties in the presence of organic substrates, and detailed NMR spectroscopic study. See DOI: 10.1039/c9na00769e

<sup>‡</sup> These authors contributed equally.


spectrum of interaction strengths. Furthermore, we have compared the case of isotropic Ncs and of monocrystalline nanorods that grow along the *c* crystallographic axis.

## Results

### Preparation of ZnO Ncs

ZnO Ncs were efficiently synthesized following an organometallic procedure that was previously reported by us.<sup>8</sup> This strategy consists in the controlled hydrolysis of a dicyclohexyl zinc precursor,  $[\text{Zn}(\text{Cy})_2]$ , in the presence of alkyl-amine ligands (here dodecyl amine – DDA). ZnO Ncs with an aspect ratio close to 1 (isotropic) were typically obtained when  $[\text{Zn}(\text{Cy})_2]$  and one equivalent of DDA were dissolved in THF under an inert atmosphere followed by the dropwise addition of a THF solution containing 2 equiv. of water at room temperature. The reaction was stirred overnight and protected from light to quantitatively yield well-defined ZnO Ncs of about 6.8 (0.7) nm in diameter (Fig. 1 and SI1†). ZnO Ncs with an aspect ratio  $\gg 1$

(nanorods) were prepared by mixing  $[\text{Zn}(\text{Cy})_2]$  with 2 equiv. of DDA followed by slow diffusion of 2 equiv. of water vapor for 4 days without any solvent. In the latter case, ZnO Ncs were quantitatively obtained with lengths ranging from 10 to 130 nm and a diameter of 4.5 (0.5) nm (Fig. 1 and SI1†).

### Optical characterization

Both samples display typical UV-visible absorption spectra with strong absorption between 300 and 375 nm ( $\approx 3.31\text{--}4.14$  eV) displaying a band gap around 363 nm (ref. 10) (Fig. 1).<sup>11</sup> This absorption is in agreement with that of nano-sized particles of ZnO displaying a band gap of  $\approx 3.40$  eV (365 nm). The emission spectra of ZnO NPs display two emission bands. The first emission band is observed in the ultra-violet region and corresponds to the direct recombination of electrons from the conduction band with holes from the valence band. This so-called excitonic emission is usually observed around 370 nm ( $\approx 3.35$  eV).<sup>12</sup> A second emission band is found in the visible region between 500 and 600 nm ( $\approx 2.48\text{--}2.07$  eV). The origin of

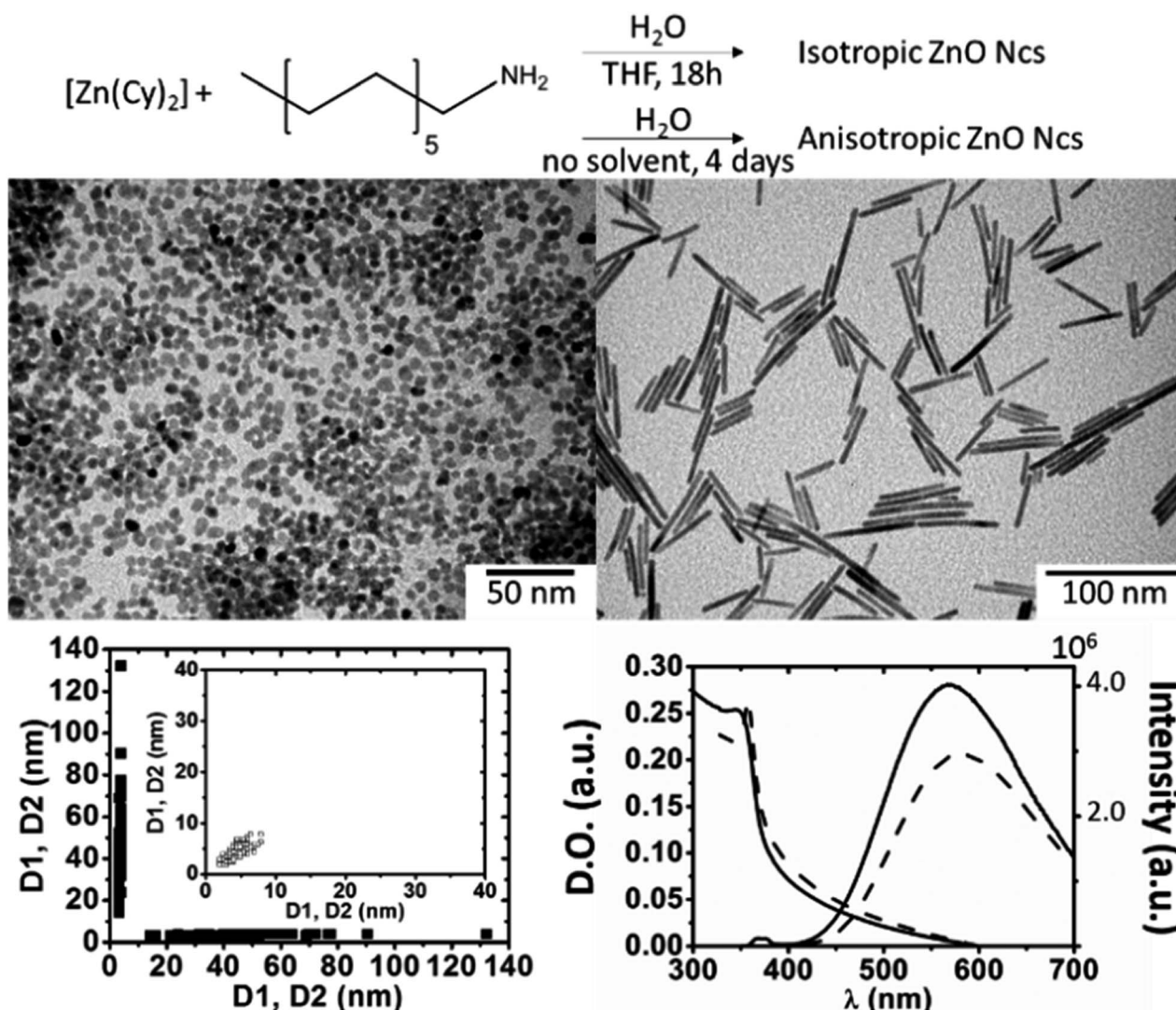


Fig. 1 Synthesis conditions, TEM images, 2D plot size,<sup>9</sup> and optical properties (absorbance and emission: excitation wavelength = 340 nm) of isotropic NPs (open squares and solid lines) and nanorods (filled squares and dashed lines).



this emission band is generally attributed to localized defects and strongly depends on the synthetic strategies; however, its origin is still under debate: oxygen vacancies ( $V_O$ ),<sup>13</sup> zinc vacancies ( $V_{Zn}$ ),<sup>14</sup> oxygen interstitials ( $O_i$ ),<sup>15</sup> zinc interstitials ( $Zn_i$ ),<sup>16</sup> and antisite oxygen ( $O_{Zn}$ ) are proposed.<sup>15,17</sup> In our case, the ZnO Ncs showed one broad band in the visible region centred at 570–580 nm ( $\approx 2.16$  eV) for excitation ranging from 280 to 360 nm ( $\approx 4.43$ – $3.45$  eV), as shown in Fig. 1 (see Optical characterization in the ESI and Fig. SI2†).<sup>18</sup> This emission is generally related specifically to oxygen vacancies which create an intermediate emissive state in the band gap. Van Dijken *et al.* explained the phenomenon at the origin of such an emission by the recombination of a shallowly trapped electron with a deeply

trapped hole.<sup>13a</sup> From the molecular point of view, this corresponds to under-coordinated zinc atoms. When donor substrates are present, they fill the incomplete coordination sphere of the zinc atoms (*i.e.* dangling bonds are removed), and the emission is quenched (*i.e.* the emissive state is suppressed or, at least, these shallow surface levels become completely inactive).

### Luminescence properties in the presence of organic substrates

The absorbance and the emission spectra of the ZnO Ncs in the presence of increasing amounts of the various organic

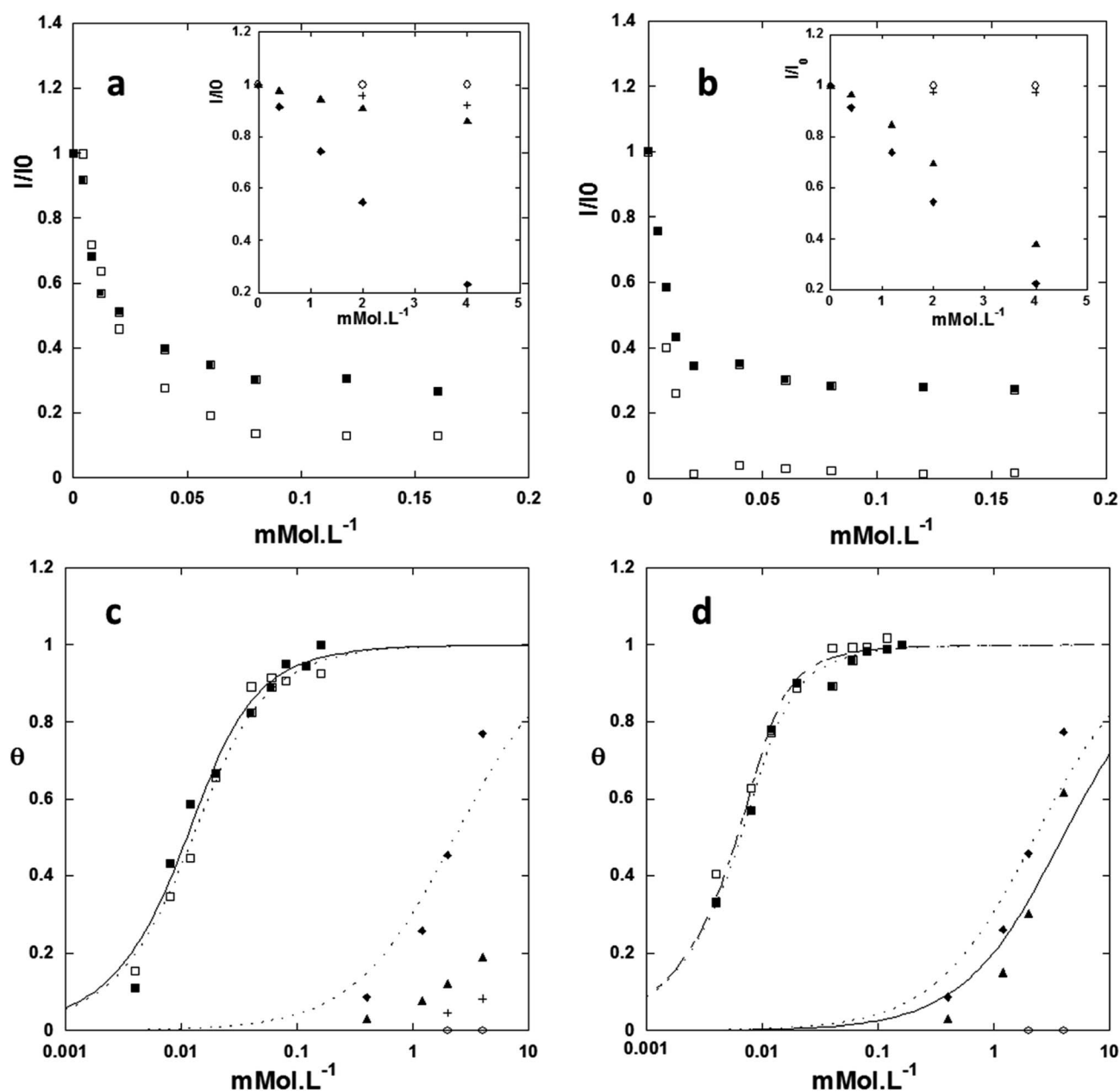


Fig. 2 Normalized emission of (a) isotropic and (b) anisotropic ZnO NPs in the presence of ligands: (■) dodecanethiol, (□) tetradecylphosphonic acid, (◆) lauric acid, (▲) hexanal, (○) hexanone, and (+) octanol; Langmuir adsorption isotherms and corresponding fit of (c) isotropic NPs and (d) nanorod ZnO NPs.



substrates were recorded under the same experimental conditions and with a constant concentration of ZnO in THF set at  $[C_{\text{ZnO}}] = 4 \times 10^{-4} \text{ mol L}^{-1}$  (for details see the Experimental section). Fig. 2a and b show the evolution of the emission intensity as a function of the amount of organic molecules added.<sup>19</sup> Three typical behaviors can be distinguished regardless of the aspect ratio of the ZnO Ncs. (1) For octanethiol and dodecanethiol species, a strong decrease of the emission is observed while the absorption properties remain unchanged (see Luminescence properties in the presence of organic substrates in the ESI and Fig. SI3–SI5†). At a high ligand concentration a residual emission is observed. The corresponding plateau value is equal to *ca.* 30% regardless of the sample. Note that similar results are obtained regardless of the length of the alkyl chain. Similarly to alkyl-thiol species, the addition of alkyl phosphonic acids induces a strong loss of emission intensity (Fig. 2 and SI6–SI8†). In this case, precipitation of the ZnO Ncs is observed beyond 40  $\mu\text{M}$  of alkyl phosphonic acid is added. The emission spectra were normalized by the amount of NPs remaining in the supernatant. However, this is only qualitative and it seems obvious that the lower plateau value compared to that of alkyl thiol is due to this precipitation. (2) The second type of behavior corresponds to molecules that lead to only small modifications of the emission intensity (typically in alkyl carboxylic acid species (Fig. SI9†) and in an even weaker way alkyl-aldehyde (Fig. SI10†)). In this case, the plateau value is not reached even for concentrations at least 100 times higher than the one needed for alkyl-thiols or alkyl-phosphonic acids. (3) Finally, the third type corresponds to the molecules that have no sensitive effect on the optical properties of the ZnO Ncs, namely alkyl-ketones (Fig. SI11†) and alkyl-alcohols (Fig. SI12†). The ligand adsorption isotherms, representing the fraction of bound sites ( $\theta$ ) as a function of the concentration of added ligands, are presented in Fig. 2c and d, assuming that (1) the residual luminescence emission is related

to core emitters which are not affected by surface bound ligands and (2) the surface emission is proportional to the fraction of unquenched surface emitters  $\theta$ , *i.e.*  $\theta = (I - I_{\text{plateau}})/(I_0 - I_{\text{plateau}})$  (Fig. 2). Fitting of the adsorption isotherms with a Langmuir model allows the determination of the number of emitting surface sites, the affinity constants of the different organic substrates for the ZnO Ncs ( $K$ ), and the residual emission (Table 1). Note that these affinity constants are in fact apparent constants, related to the quenching of luminescence. Thus, the measured apparent constant of a substrate that binds to the nanoparticle surface with a limited quenching effect would be low. The apparent binding constants are high for thiols and phosphonic acids (in the range of 100–700  $\text{mM}^{-1}$ ). They are 4 orders of magnitude smaller for carboxylic acids, and even smaller (hexanal) or not measurable for the other substrates (hexanone and octanol).

The number of binding sites is found to be 0.012 mM, and hence 0.030 sites per Zn atom for isotropic NPs,<sup>20</sup> consistent with previous results.<sup>21</sup> It is slightly lower for the nanorods (0.010 mM, and thus 0.025 sites per Zn atom). The difference in the determined number of binding sites between isotropic Ncs and rods is correlated with the difference of the total surface (see Table SI1†). Indeed, for the same volume, isotropic Ncs typically exhibit a surface excess of 20% compared to rods. Therefore, this shows that the substrates bind to both the basal and lateral surfaces. However, for phosphonic acids and thiols, which bind strongly to the Ncs, the affinity constant is *ca.* 3 to 4 times higher in the case of the rods than in the case of the isotropic ZnO Ncs. This geometrical effect may be due to different enthalpies of interactions of the functional groups of the substrates with the two types of surfaces (*i.e.* basal and lateral ones). In addition, the van der Waals interactions between the alkyl chain groups of adsorbed substrates on the lateral faces may be more favourable in the case of the nanorods, owing to lower global curvature.

**Table 1** Number of emitting surface sites, apparent affinity constants ( $K$ ), and residual emission of both isotropic Ncs and nanorods for the different organic substrates

Organic substrate	Isotropic nanorod	Surface sites (mM)	$K$ ( $\text{mM}^{-1}$ )	Residual emission (%)
Dodecanethiol	Iso	$0.012 \pm 0.004$	$192 \pm 66$	27
	Rods	$0.010 \pm 0.001$	$668 \pm 174$	26
Octanethiol	Iso	$0.012^a$	$185 \pm 30$	27
	Rods	$0.010^a$	$535 \pm 126$	26
Tetradecyl phosphonic acid	Iso	$0.012^a$	$153 \pm 16$	12.8
	Rods	$0.010^a$	$950 \pm 146$	1.5
Hexyl phosphonic acid	Iso	$0.012^a$	$183 \pm 30$	12.8
	Rods	$0.010^a$	$790 \pm 95$	1.5
Lauric acid	Iso	$0.012^a$	$0.44 \pm 0.10$	n.d.
	Rods	$0.010^a$	$0.44 \pm 0.10$	n.d.
Hexanal	Iso	n.d.	n.d.	n.d.
	Rods	$0.010^a$	$0.25 \pm 0.06$	n.d.
Hexanone	Iso	n.d.	n.d.	n.d.
	Rods	n.d.	n.d.	n.d.
Octanol	Iso	n.d.	n.d.	n.d.
	Rods	n.d.	n.d.	n.d.

<sup>a</sup> Fixed fit parameters.





## NMR study

The interaction of the various substrates with the surface of the ZnO Ncs was characterized using both liquid and solid state NMR spectroscopy. The solution made of ZnO Ncs stabilized by DDA molecules, namely ZnO/DDA, was the starting point and the measurements were performed under the same experimental conditions *i.e.* 1 equiv. of a given substrate relative to DDA was added to the pristine ZnO/DDA colloidal solution. Fig. 3 and 4 show the evolution of the  $^1\text{H}$  and  $^{13}\text{C}$  CPMAS NMR spectra, respectively, when the different organic substrates are added into the pristine ZnO/DDA colloidal solution (see the NMR spectroscopic study in the ESI for details and Fig. SI13–SI15† for the full scale evolution of the  $^1\text{H}$  NMR spectra, the diffusion filtered  $^1\text{H}$  NMR spectra, and the  $^{13}\text{C}$  CPMAS NMR spectra, respectively). In the ZnO/DDA solution, two different kinds of DDA molecules interacting with the ZnO Ncs are observed, as previously reported.<sup>7</sup> One is strongly bonded to ZnO Ncs and corresponds to DDA in the first ligand shell surrounding the ZnO Ncs while the second one weakly interacts with the NPs and forms the second ligand shell (see the NMR spectroscopic study in the ESI for details and Fig. SI16 and SI17†).

After addition of an organic substrate, three behaviors can be distinguished regardless of the aspect ratio of the ZnO NPs. (1) For thiols, phosphonic acids, and carboxylic acid species, the NMR study evidences that these substrates are present in the first ligand shell of the ZnO Ncs (see the NMR spectroscopic study for details and Fig. SI18–SI20† for thiols, Fig. SI21–SI23† for phosphonic acids, and Fig. SI24† for carboxylic acids). Thiols and phosphonic acids are strongly bound to the ZnO Ncs while carboxylic acid interacts as an ammonium-carboxylate ion-pair; (2) alcohols and aldehydes interact with the ZnO Ncs only through the second ligand shell while (3) ketones have no interaction (see the NMR spectroscopic study in the ESI for details and Fig. SI25 and SI26† for alcohols, Fig. SI27–SI30† for

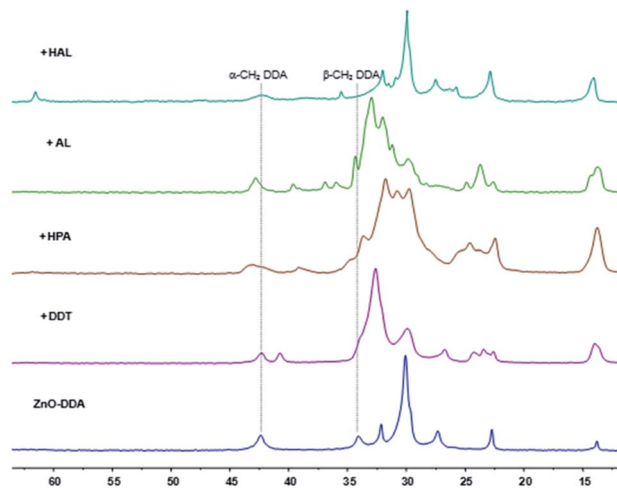
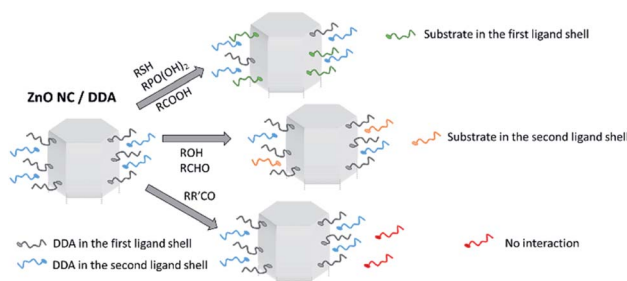


Fig. 4  $^{13}\text{C}$  CPMAS NMR spectra (in the 70–10 ppm area) of ZnO–DDA and with addition of dodecanethiol (DDT), hexylphosphonic acid (HPA), lauric acid (AL) and hexanal (HAL).



Scheme 1 Schematic view of the three behaviors observed after the addition of one of the various organic substrates. Illustration of the first and second ligand shell interaction of the substrate with the ZnO Ncs.

aldehydes, and Fig. SI31 and SI32† for ketones). Note that when hexanal is introduced in the ZnO/DDA colloidal solution, imine molecules are formed *via* the well-known condensation reaction between DDA and hexanal (see Fig. SI27†).<sup>19</sup> The  $^1\text{H}$  NOESY experiment (Fig. SI29†) reveals that these imines weakly interact with ZnO NPs (*i.e.* in the second ligand shell). Scheme 1 illustrates these results.

## Discussion

To understand the behavior of the system towards the various substrates, we should consider the interaction of the substrates not only with ZnO but with the overall ZnO/DDA system. This necessitates the discussion on the interactions of the six families of substrates with the ZnO/DDA colloids. Let's recall that only thiols, phosphonic acids, and carboxylic acids – the substrates for which the NMR studies evidence that they interact within the first ligand shell of the ZnO/DDA system – lead to a modification of the emission properties. Among these substrates, thiols and phosphonic acids lead to an efficient quenching of the emission while for the carboxylic acid it is moderate.

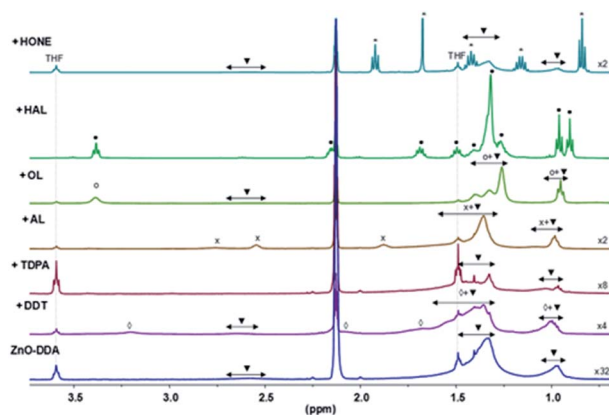


Fig. 3 Evolution of the 3.6–0.7 ppm area of the  $^1\text{H}$  NMR spectrum (Tol- $\text{d}_3$ ; 296 K) when different organic substrates are added in the pristine ZnO/DDA colloidal solution of ZnO/DDA (▼): dodecanethiol (DDT, ◇), tetradecylphosphonic acid (TDPA), lauric acid (AL), octanol (OL, ○), hexanal (HAL) and hexan-2-one (HONE, \*). × and ● indicate the resonances of carboxylate-ammonium and imine molecules that appear when carboxylic acid or alkyl-aldehyde are added, respectively.



The six families of substrates investigated here present a wide range of  $pK_a$  values spanning from 2 to 24: phosphonic acids (which are diacids, 2 and 7), carboxylic acids (5), thiols (10), aldehydes (or imines) (14 or 24 respectively), alcohols (16), and ketones (20). It is remarkable that the substrates for which the emission properties are modified (thiols, carboxylic acids, and phosphonic acids) have  $pK_a$  values lower than that of DDA ( $pK_a = 11$ ) and are therefore deprotonated in the presence of DDA. Once deprotonated, these substrates possess a stronger ligand character for Zn centers. It is very likely that coordination will occur preferentially with the zinc atoms that are under-coordinated, *i.e.* at the emissive defect sites (oxygen vacancies) and result in an efficient quenching of the emission. The interaction (or not) of a given substrate will therefore be determined by its  $pK_a$  versus the  $pK_a$  of DDA.

The hard or soft character of the substrates enables us to fully understand the influence of the substrate on the emission intensity. In Pearson's hard and soft (Lewis) acid and base (HSAB) concept, hard (soft) donor species strongly bind to hard (soft) acceptors. With this in mind, we expect thiolates and phosphites, which are soft donors,<sup>22</sup> to bind strongly to the rather soft zinc.<sup>23</sup> As mentioned above, this will occur preferentially where the zinc atoms are under-coordinated and will result in an efficient quenching of the emission. For the carboxylate substrates, which are hard donors, even though Zn cations could accommodate them, NMR data clearly reveal that the carboxylates observed within the first ligand shell interact as ammonium-carboxylate ion pairs with the Nc surface. It is very likely that carboxylate will predominantly associate with the NP surface *via* hydrogen bonding with the hydroxyl group. Therefore coordination with Zn remains limited resulting in a moderate quenching of the emission. This is fully consistent with the apparent affinity constants (Table 1) determined from luminescence measurements. For thiol and phosphonic acid substrates, the affinity constant is found to be at least three orders of magnitude larger than for the other substrates.

## Conclusions

The gathered results show that the analysis of substrate–ZnO/DDA interactions in terms of  $pK_a$  and HSAB theory provides new insights into the metal–ligand interactions at the molecular level thus laying the basis for a rationale for the observed luminescence properties. In addition, the measurements of the affinity constants represent an important step towards the prediction of ligand binding and ligand exchanges, as well as colloidal stability of NPs. Finally, this systematic approach can be straightforwardly extended towards sister oxide materials or even other nanoobjects, nanocatalysts, *etc.*

## Experimental section

### Materials and reagents

Zinc dicyclohexyl [ $Zn(Cy)_2$ ] was purchased from Nanomeps and stored in a glove box at  $-25\text{ }^\circ\text{C}$ . Dodecylamine (DDA) was obtained from Aldrich and stored in a glove box. Organic molecules such as dodecanethiol (DDT), octanethiol (OT),

hexylphosphonic acid (HPA), tetradecylphosphonic acid (TDPA), lauric acid (AL), hexanal (HAL), hexan-2-one (HONE) and octanol (OL) were purchased from Aldrich and used as received. The preparation of ZnO nanodisks (S1) and ZnO nanorods (S2) was carried out under an oxygen-free argon atmosphere using standard Schlenk and glove box techniques. Tetrahydrofuran (THF) was dried using an MBraun SPS column.

### Preparation of ZnO nanodisks S1

$Zn(Cy)_2$  (231.7 mg, 1 mmol) and DDA (185.4 mg, 1 mmol) were introduced in a Schlenk flask and 12 mL of THF was added. The solution was then stirred under argon and protected from light before dropwise addition of 0.46 mL of a THF solution containing 36  $\mu\text{L}$  of  $H_2O$  (2 mmol). After 18 h, the stock solution was prepared for the optical measurements with the concentration of ZnO set at  $8 \times 10^{-4}\text{ mol L}^{-1}$  and was used within one week.

### Preparation of ZnO nanorods S2

$Zn(Cy)_2$  (231.7 mg, 1 mmol) and DDA (368.8 mg, 1 mmol) were mixed under argon followed by slow diffusion of 36  $\mu\text{L}$  of water vapor for 4 days. The stock solution for the optical measurements was  $8 \times 10^{-4}\text{ mol L}^{-1}$  ZnO and was used within one week.

### Transmission electron microscopy

Samples for TEM studies were prepared by slow evaporation of droplets of the colloidal solution deposited on carbon-supported copper grids. The samples were dried overnight under vacuum ( $5 \times 10^{-4}$  mbar) with a BOC Edward turbomolecular pump. The TEM experiments were performed at the "Service Commun de Microscopie de l'Université Paul Sabatier" TEMSCAN on a JEOL JEM1011 electron microscope operating at 100 kV with a resolution of 0.45 nm. The nanoparticle size-distribution histograms were determined by using magnified TEM images. The size distribution of the particles was determined by measuring a minimum of 250 particles for each sample. The size distributions observed were fitted with Gaussian curves.

### Optical measurements

All optical measurements were carried out at room temperature (298 K) using quartz cells with an optical pathway of 1 cm. Absorbance spectra were recorded on a PerkinElmer Lambda 35 spectrophotometer between 280 and 600 nm. Emission spectra were measured using a Horiba-Jobin Yvon FluoroMax-4 spectrofluorometer, equipped with three-slit double-grating excitation and emission monochromators. Measurement were performed on a Horiba-Jobin Yvon FluoroMax-4 spectrofluorometer. Slits were kept constant and set at 2.2/3.5 nm for emission/excitation slits, respectively. The excitation wavelength was fixed at 340 nm and the emission spectra were recorded between 350 and 700 nm. An emission band-pass filter of 370 nm was used. Spectra were reference-corrected for both the excitation source light-intensity variation (lamp and grating) and the emission spectral response (detector and grating).



Samples for fluorescence experiments were prepared in a 10 mL volumetric flask with a constant concentration of  $4 \times 10^{-4} \text{ mol L}^{-1}$  ZnO/DDA in THF. Typically, 5 mL of a freshly prepared stock solution at  $8 \times 10^{-4} \text{ mol L}^{-1}$  ZnO/DDA was placed in a 10 mL volumetric flask followed by addition of an appropriate amount of the organic substrate (e.g. for addition of 0.02 equiv. of dodecanethiol,  $n = 8 \times 10^{-6} \text{ mol}$ , 50  $\mu\text{L}$  of a stock solution of  $1.6 \times 10^{-3} \text{ mol L}^{-1}$  dodecanethiol in THF was added to the 10 mL volumetric flask). Thereafter, the volumetric flask was filled with THF and an approximately 4 mL aliquot was placed in quartz cells prior to recording UV-visible and fluorescence spectra.

### Nuclear magnetic resonance spectroscopy

1D and 2D  $^1\text{H}$  and  $^{13}\text{C}$  liquid state NMR spectra were recorded on a Bruker Avance 500 spectrometer equipped with a 5 mm triple resonance inverse Z-gradient probe. Samples were prepared in toluene- $d_8$ .  $^1\text{H}$  and  $^{13}\text{C}$  signals were assigned on the basis of chemical shifts, spin-spin coupling constants, splitting patterns and signal intensities, and by using  $^1\text{H}$ - $^1\text{H}$  TOCSY,  $^1\text{H}$ - $^{13}\text{C}$  HMQC and  $^1\text{H}$ - $^{13}\text{C}$  HMBC experiments. The 2D NOESY measurements were performed with a mixing time of 100 ms. Diffusion measurements were carried out using the stimulated echo pulse sequence with bipolar gradient pulses. The diffusion dimension was processed with the Laplace inversion routine CONTIN (Topspin software). 1D solid state NMR spectra were recorded on a Bruker AvanceIII 400 spectrometer. Samples were packed into 4 mm zirconia rotors inside a glove box. The rotors were spun at 8 or 10 kHz at 293 K.  $^{13}\text{C}$  MAS with Direct Polarization (DP) was performed with a small flip angle of  $30^\circ$  and a recycle delay of 10 s.  $^{13}\text{C}$  and  $^{31}\text{P}$  with Cross Polarization (CP) were performed with a recycle delay of 2 s and a contact time of 2 ms.  $^1\text{H}$  and  $^{13}\text{C}$  chemical shifts were relative to TMS and  $^{31}\text{P}$  chemical shifts were referenced to an external 85%  $\text{H}_3\text{PO}_4$  sample.

### Conflicts of interest

There are no conflicts to declare.

### Acknowledgements

The authors wish to acknowledge the financial support from the Centre National de la Recherche Scientifique (CNRS).

### Notes and references

- (a) Y. Chen, Y. Xianyu and X. Jiang, *Acc. Chem. Res.*, 2017, **50**, 310–319; (b) Q. M. Kainz and O. Reiser, *Acc. Chem. Res.*, 2014, **47**, 667–677.
- (a) L. Malassis, R. Dreyfus, R. J. Murphy, L. A. Hough, B. Donnio and C. B. Murray, *RSC Adv.*, 2016, **6**, 33092–33100; (b) J. Rubio-Garcia, A. Dazzazi, Y. Coppel, P. Mascalchi, L. Salome, A. Bouhaouss, M. L. Kahn and F. Gauffre, *J. Mater. Chem.*, 2012, **22**, 14538–14545.
- A. Glaria, M. L. Kahn, B. Chaudret, P. Lecante, M. J. Casanove and B. Barbara, *Mater. Chem. Phys.*, 2011, **129**, 605–610.
- (a) W. Ma, L. Xu, A. F. de Moura, X. Wu, H. Kuang, C. Xu and N. A. Kotov, *Chem. Rev.*, 2017, **117**, 8041–8093; (b) H. Kang, J. T. Buchman, R. S. Rodriguez, H. L. Ring, J. He, K. C. Bantz and C. L. Haynes, *Chem. Rev.*, 2019, **119**, 664–699; (c) G. Spataro, A. Dazzazi, S. Fortuny, Y. Champouret, Y. Coppel, J. Rubio-Garcia, A. Bouhaouss, F. Gauffre and M. L. Kahn, *Eur. J. Inorg. Chem.*, 2016, 2056–2062, DOI: 10.1002/ejic.201501186.
- (a) L. Xu, H.-W. Liang, Y. Yang and S.-H. Yu, *Chem. Rev.*, 2018, **118**, 3209–3250; (b) S. Mourdikoudis and L. M. Liz-Marzan, *Chem. Mater.*, 2013, **25**, 1465–1476; (c) X. Hu and S. Dong, *J. Mater. Chem.*, 2008, **18**, 1279–1295; (d) I. Hussain, N. B. Singh, A. Singh, H. Singh and S. C. Singh, *Biotechnol. Lett.*, 2016, **38**, 545–560; (e) D. Ling, M. J. Hackett and T. Hyeon, *Nano Today*, 2014, **9**, 457–477; (f) M. H. G. Precht and P. S. Campbell, *Nanotechnol. Rev.*, 2013, **2**, 577–595; (g) J. Rubio-Garcia, Y. Coppel, P. Lecante, C. Mingotaud, B. Chaudret, F. Gauffre and M. L. Kahn, *Chem. Commun.*, 2011, **47**, 988–990; (h) G. L. Drisko, C. Gatel, P.-F. Fazzini, A. Ibarra, S. Mourdikoudis, K. Fajerwerg, P. Fau and M. L. Kahn, *Nano Lett.*, 2018, **18**, 1733–1738; (i) S. Mourdikoudis, V. Colliere, P. Fau and M. L. Kahn, *Dalton Trans.*, 2014, **43**, 8469–8479.
- (a) M. L. Kahn, A. Glaria, C. Pages, M. Monge, L. Saint Macary, A. Maisonnat and B. Chaudret, *J. Mater. Chem.*, 2009, **19**, 4044–4060; (b) J. Jonca, A. Ryzhikov, M. L. Kahn, K. Fajerwerg, A. Chapelle, P. Menini and P. Fau, *Chem.–Eur. J.*, 2016, **22**, 10127–10135; (c) J. Jonca, A. Ryzhikov, S. Palussiere, J. Esvan, K. Fajerwerg, P. Menini, M. L. Kahn and P. Fau, *ChemPhysChem*, 2017, **18**, 2658–2665.
- Y. Coppel, G. Spataro, C. Pages, B. Chaudret, A. Maisonnat and M. L. Kahn, *Chem.–Eur. J.*, 2012, **18**, 5384–5393.
- (a) M. Monge, M. L. Kahn, A. Maisonnat and B. Chaudret, *Angew. Chem., Int. Ed.*, 2003, **42**, 5321–5324; (b) M. L. Kahn, M. Monge, V. Colliere, F. Senocq, A. Maisonnat and B. Chaudret, *Adv. Funct. Mater.*, 2005, **15**, 458–468.
- Z. H. Zhao, Z. Q. Zheng, C. Roux, C. Delmas, J. D. Marty, M. L. Kahn and C. Mingotaud, *Chem.–Eur. J.*, 2016, **22**, 12424–12429.
- $\lambda_{1/2}$  is the inflection point calculated by differentiation of the absorption spectrum or the wavelength at which the absorption is half of that at the excitonic peak or shoulder.
- (a) E. A. Meulenkaamp, *J. Phys. Chem. B*, 1998, **102**, 5566–5572; (b) L. Zhang, L. Yin, C. Wang, N. Iun, Y. Qi and D. Xiang, *J. Phys. Chem. C*, 2010, **114**, 9651–9658.
- F. H. Leiter, H. R. Alves, N. G. Romanov, D. M. Hofmann and B. K. Meyer, *Physica B*, 2003, **340–342**, 201–205.
- (a) A. v. Dijken, E. A. Meulenkaamp, D. Vanmaekelbergh and A. Meijerink, *J. Phys. Chem. B*, 2000, **104**, 1715–1723; (b) A. v. Dijken, J. Makkinje and A. Meijerink, *J. Lumin.*, 2001, **92**, 323–328; (c) A. v. Dijken, E. A. Meulenkaamp, D. Vammaekelberg and A. Meijerink, *J. Lumin.*, 2000, **90**, 123–128; (d) Z. Y. Xue, D. H. Zhang, Q. P. Wang and J. H. Wang, *Appl. Surf. Sci.*, 2002, **195**, 126–129.



- 14 (a) Y. W. Heo, D. P. Norton and S. J. Pearton, *J. Appl. Phys.*, 2005, **98**, 073502; (b) Q. X. Zhao, P. Klason, M. Willander, H. M. Zhong, W. Lu and J. H. Yang, *Appl. Phys. Lett.*, 2005, **87**, 211912.
- 15 (a) X. Liu, X.-H. Wu, H. Cao and R. P. H. Chang, *J. Appl. Phys.*, 2004, **95**, 3141–3147; (b) D. Li, Y. H. Leung, A. B. Djurišić, Z. T. Liu, M. H. Xie, S. L. Shi, S. J. Xu and W. K. Chan, *Appl. Phys. Lett.*, 2004, **85**, 1601.
- 16 (a) B. Lin, Z. Fu and Y. Jia, *Appl. Phys. Lett.*, 2001, **79**, 943; (b) Q. Yang, K. Tang, J. Zuo and Y. Qin, *Appl. Phys. A: Mater. Sci. Process.*, 2004, **79**, 1847–1851.
- 17 D. S. Bohle and C. J. Spina, *J. Am. Chem. Soc.*, 2009, **131**, 4397–4404.
- 18 M. L. Kahn, T. Cardinal, B. Bousquet, M. Monge, V. Jubera and B. Chaudret, *ChemPhysChem*, 2006, **7**, 2392–2397.
- 19 K. P. C. Vollhardt and N. E. Schore, *Organic Chemistry: Structure and Function*, W. H. Freeman, New York, 5th edn, 2007.
- 20 0.4 mM Zn atoms and 0.012 mM binding sites leads to 010.003 eq. per Zn atom.
- 21 J. Massaad, Y. Coppel, M. Sliwa, M. L. Kahn, C. Coudret and F. Gauffre, *Phys. Chem. Chem. Phys.*, 2014, **16**, 22775–22783.
- 22 K. B. Nilsson, M. Maliarik, I. Persson and M. Sandström, *Dalton Trans.*, 2008, 2303–2313.
- 23 R. G. Pearson, *J. Chem. Educ.*, 1968, **45**, 581–587.

